Elsevier Editorial System(tm) for Materials and Design
Manuscript Draft

Manuscript Number: JMAD-D-13-02480R3

Title: EXPERIMENTAL AND NUMERICAL MODELLING OF BASALT TEXTILE REINFORCED MORTAR BEHAVIOR UNDER UNIAXIAL TENSILE STRESS

Article Type: Original Article

Keywords: Basalt; Modelling; Mortar; Numerical; Tensile; Textile.

Corresponding Author: Dr. Pello Larrinaga Alonso, Ph. D.

Corresponding Author's Institution: TECNALIA Research & Innovation

First Author: Pello Larrinaga Alonso, Ph. D.

Order of Authors: Pello Larrinaga Alonso, Ph. D.; Carlos Chastre, Associated Professor; Hugo C Biscaia, PhD Civil Engineer; José Tomás San-José, Associated Professor

Abstract: During the last years several projects and studies have improved the knowledge about Textile Reinforced Mortar technology. TRM has already been used in strengthening masonry and reinforced concrete structural elements such as walls, arches, columns and beams. This material is presented as a real alternative to the use of fibre-reinforced polymers (FRP) in situations where these composites have presented some drawbacks or their use is banned. Textile Reinforced Mortar show a complex mechanical behaviour derived from the heterogeneity of the constituent materials. This paper aims to deepen the knowledge of this composite material in terms of tensile behaviour.
Following this scope, this paper presents an experimental campaign focused on thirty one TRM specimens reinforced with four different reinforcing ratios. The results are analysed and contrasted with two distinct models. i) the Aveston-Cooper-Kelly theory (ACK) which is based on a tri-linear analytical approach; and ii) a nonlinear numerical simulation with a 3D Finite Element code.
The FEA of the TRM tensile tests also showed no significant dependence on the basalt-to-mortar interface, i.e., the choice of a bond-slip curve in order to reproduce the bond stresses and slippages along the interface is irrelevant and it can be simply considered as rigid interface.

Making more deepen the knowledge of Textile Reinforced Mortar in tensile stress → Analysing the effect of the reinforcing ratio of the composite → To compare results with Aveston-Cooper-Kelly theory → To develop a numerical model based on a Finite Element code → Considering the importance of the bond-slip law of the mortar-to-textile-interface.

EXPERIMENTAL AND NUMERICAL MODELLING OF BASALT TEXTILE REINFORCED MORTAR BEHAVIOR UNDER UNIAXIAL TENSILE STRESS

Pello Larrinaga[1]*, Carlos Chastre[2], Hugo C. Biscaia [2], José T. San-José[3]

Abstract

During the last years several projects and studies have improved the knowledge about Textile Reinforced Mortar (TRM) technology. TRM has already been used in strengthening masonry and reinforced concrete structural elements such as walls, arches, columns and beams. This material is presented as a real alternative to the use of fibre-reinforced polymers (FRP) in situations where these composites have presented some drawbacks or their use is banned. Textile Reinforced Mortar show a complex mechanical behaviour derived from the heterogeneity of the constituent materials. This paper aims to deepen the knowledge of this composite material in terms of tensile behaviour.

Following this scope, this paper presents an experimental campaign focused on thirty one TRM specimens reinforced with four different reinforcing ratios. The results are analysed and contrasted with two distinct models. i) the Aveston-Cooper-Kelly theory (ACK) which is based on a tri-linear analytical approach; and ii) a nonlinear numerical simulation with a 3D Finite Element code.

The Finite Element Analysis (FEA) of the TRM tensile tests also showed no significant dependence on the basalt-to-mortar interface, i.e., the choice of a bond-slip curve in order to reproduce the bond stresses and slippages along the interface is irrelevant and it can be simply considered as rigid interface.

Keywords: Basalt; Modelling; Mortar; Numerical; Tensile; Textile.

1. Introduction

Composites of technical textiles acting as reinforcement and cement-based mortars used as matrices, called Textile Reinforced Mortar (TRM), provide the opportunity to strengthen existing reinforced concrete structures in flexure, shear and confinement. The effect of TRM as strengthening technology has been successfully proven by several research projects [1-5]. However, its implementation as a regular technique is still far.

[1] TECNALIA. c/Geldo, Parque Tecnológico de Bizkaia, Ed. 700, 48160, Derio, Spain.
[2] UNIC, Faculdade de Ciências e Tecnologia, Universidade Nova de Lisboa, 2829-516 Caparica – Portugal
[3] UPV/EHU, Department of Engineering Materials. c/Alamaeda Uquijo s/n, 48012, Bilbao, Spain

* Corresponding author. Tel: +34 667 178 992/946 430 850; fax: +34 946 460 900
E-mail address: pello.larrinaga@tecnalia.com

One important step to reach this objective is modelling the mechanical behaviour of TRM for future numerical applications in real situations.

The tensile behaviour of cement-based composites is different from that of polymeric matrices due to the brittleness of the inorganic matrix, i.e. the ultimate strain in tension of these materials is considerably smaller than that of the fibres. In fibro-plastic composites (FRP), the matrix presents a more ductile behaviour than fibres. Because of this, organic composites present elastic behaviour up to the point of failure (if the fibres are elastic up to failure too). On the other hand, inorganic matrices crack before the maximum strain of the textile is reached. Hence, the reinforcement becomes effective when the matrix starts to develop cracks. After cracking, the tensile stress within the cracked cross-section is carried entirely by the internal reinforcement. To achieve this effect a minimum volume of fibres is required, and then, the composite would be able to resist the imposed load. The critical volume content of the fibres in cement composites is established at about 1-3% in volume. [6].

The stress-strain diagram of TRM under uniaxial loading is presented in Fig. 1. The non-linear curve is divided into three stages [7, 8]. A brief description of the stress-strain plotted curve is given below.

Fig. 1. Stress-strain relationship of TRM under uniaxial tension.

Stage I ends at the point where the first crack appears ($\varepsilon_{t,I}$). The stiffness of the uncracked composite material is dependent on the stiffness of the mortar. This stage is known as pre-cracking stage.

When the mortar tensile strength is exceeded, the first crack is formed and the whole tensile force is carried by the textile reinforcement, which must be able to resist the acting load. With the increase of the tensile force, new cracks appear in the specimen. Due to the bond between rovings and mortar, forces are initiated again in the matrix. When the tensile strength of the cementitious mortar is reached once more, a new crack is formed. The distance between cracks and their width is influenced by the reinforcement material, the reinforcing rate, the reinforcement-matrix bond characteristics and the tension failure strain of the mortar [8]. Stage II, also known as multiple cracking stage, ends when no further cracks can occur ($\varepsilon_{t,II}$).

Stage III (post-cracking stage) is characterized by a stabilized crack pattern. When all the cracks are formed, the material behaves in a linear way again (with a lower slope than the obtained in Stage I) and only the fibres carry extra load up to the failure point of the composite ($\varepsilon_{t,III}$). The stiffness of this third stage is lower (10-30%) than the elastic modulus of the textile reinforcement (not that of the fibres) [9]. Hence, the stage III curve could be, approximately, parallel to the strain-stress curve of the textile under

pure tensile load. The difference is caused by two complementary factors. Firstly, the loss of adherence between the mortar and the rovings and secondly, the impossibility of the mortar to impregnate all the filaments that compose each textile roving. The roving can be divided into two groups: the outer and inner filaments. The former consists of fibres which are completely bonded to the cement-based matrix. The inner filaments has not direct contact with the mortar, the load transmission between them is determined by friction bond.

Generally, load-bearing behaviour is evaluated by means of bending or tensile tests. In ceramic and porous materials, the former are easier to perform. However, stress-strain curves obtained by means of uniaxial tensile tests provide more detailed information about the properties and real behaviour of this kind of composite material [10].

In this paper, the results of an experimental campaign are showed and analysed. Basalt, a novelty material in this field, has been selected to act as TRM reinforcement. Besides, the effect of the reinforcement rate is also studied: one to four layers were applied in the specimens. Finally, the experimental data are contrasted with the results derived from two different models: the well-known Aveston-Cooper-Kelly (ACK) theory for inorganic-based composites and a Finite Element Analysis (FEA) carried out to simulate the TRM behaviour.

2. Materials

2.1.Basalt as reinforcing material

Over recent years, carbon suppliers have found it difficult to obtain carbon fibres. In the immediate future, the amount of this material that is available may not be enough to satisfy the increasing demand of the construction industry [11]. Basalt appears to be a material which could offer interesting opportunities in the future. Recent studies have included basalt as reinforcement in FRP composites [12]. Nevertheless, it was in the TRM field where its structural application started.

Its mechanical properties are slightly better than those of glass fibres [13-15]. So, together with its low cost, it could serve as a natural replacement for glass fibre as reinforcement. The elastic tensile modulus of basalt fibres (80-110GPa) is higher than that of E-glass fibre (70-75GPa). Besides, basalt has low elongation ratios, and perfectly elastic characteristics up to the point of failure, with an ultimate strain value that is higher than 2%.

2.2.Basalt and mortar characterization

The textile applied as composite internal reinforcement consists of rovings woven in the two principal directions creating therefore a bidirectional mesh. Basalt rovings are covered by a bitumen coat in order to improve the bond between the mortar matrix and

the textile. Besides, the presence of the coat enhances the load transmission to all the roving filaments so the textile performance is improved. In Table 1 the manufacturing specifications of the basalt fibres are summarized.

Table 1
Manufacturing specifications and pure tensile behaviour of basalt (fibres and textile)

Previous studies show that there is a considerable gap between the tensile strength and Young's modulus values of a single fibre or filament and those of the textile mesh [16]. For this reason, the mechanical characteristics of the textile reinforcement material were determined in tensile tests on textile specimens whose length was 600mm. In order to carry out a suitable data acquisition, a speed of 1mm/min was chosen for the present test, influenced by the standard ASTM: D-5034. Additionally, Table 1 summarises the results obtained in the textile characterization.

Due to the difficulty of achieving an identical initial length and strain for all the strands of the specimens, it was impossible to achieve a simultaneous rupture of all the rovings. Therefore, tensile strength results and ultimate strains should not be considered as definitive values. However, the elastic modulus values obtained in this test are considered for the models included in this paper. As the tested textile presents linear behaviour until rupture, the Young's modulus for each specimen can be easily calculated [17].

The effectiveness of any externally bonded reinforcement is highly dependant on the bond between the composite and the substrate, and the interaction between the matrix and the inner reinforcement. Therefore, the interface behaviour and the mortar-reinforcement relationship are key elements for obtaining high performance of the TRM strengthening technique [18]. Besides, there are other important characteristics that the mortar should fulfil such as high workability, chemical and physical compatibility with concrete, low creep or shrinkage, permeability, sufficient shear (hence tensile) strength, resilience or flexibility to allow natural deformation and initial high strength [19].

For this study a non-commercial cement-based mortar was used as TRM matrix. The above-considered characteristics were taken into account. The maximum grain size of the sand used in the mortar was 0.6mm. This factor enhances the workability of the fresh mixture and facilitates its interaction with the fibre textile mesh. Table 2 shows the basic composition of the mortar. The amount of redispersable resins was lower than 5%, in order to achieve a fire-proof mortar. Flexural strength tests, as well as compressive tests, were performed at an age of 7 and 28 days according to [20].

Table 2
Mortar dosage by weight (%) and mechanical characterization

3. Experimental program

In total, thirty one specimens were manufactured and tested, three unreinforced and twenty eight with internal reinforcement. Test setup and specimens dimensions were influenced by previous works and considering the existing bibliography. Four series, from one to four textile layers, of seven specimens each one were defined. Hence, the effect of reinforcing rate was likewise analysed. The purpose of testing unreinforced specimens was to characterize the behaviour of the mortar until the first crack, i.e. the first stage in the TRM specimens under tensile load.

3.1.Specimens manufacturing

The specimen geometry has a relevant influence in the result of the test. Over the past few years, several geometries have been proposed [18, 21, 22]. For the present study it was decided to manufacture specimens with a 100x10mm^2 cross-sectional area and 600mm in length. Samples were prepared in plywood formworks. The ends of each specimen were reinforced with two additional layers of 200x100mm^2 textile, in order to promote the failure of the specimen in its middle third portion [4,17]. The internal layer (800x100mm^2) was positioned in the middle of the cross section. For the specimens reinforced with two or more layers, the textile pieces were placed uniformly, e.g. three layers placed every 2.5mm. In the case of the unreinforced specimens, only the additional reinforcement was installed at both ends with the aim of forcing the brittle failure in the afore-mentioned middle third portion.

Fig. 2. Geometry of a tensile specimen.

After casting, the specimens were kept in a saturated atmosphere for seven days, and were then stored for 21 days in laboratory conditions (18ºC and 60%RH). All the specimens were tested between 28 and 34 days after their construction.

3.2.Test Setup

TRM tensile specimens were placed in a Schenk 100kN press which was programmed to exert a deformation rate of 0.5mm/min [18]. The load transmission between the specimens ant the testing machine was achieved by means of designed metallic clamps. The torque applied to the clamp screws was carefully chosen, in view of possible damage to the mortar placed between the two plates.

As has been stated before, the presence of the extra textile material at the ends of the specimen forced its failure in the middle third part. The elongation of that area was recorded by means of two LVDTs; the measured length was 210mm. All the

experimental information obtained was compiled using data logger with a frequency of 5Hz. Fig. 3 provides a general view of the test.

Fig. 3. Lay-out of the uniaxial tensile test setup.

4. Experimental results

As expected, only one crack was formed in the unreinforced specimens. The basic information gathered in this series is compiled in Table 3.

Table 3
Average results of unreinforced specimens

The results of the remaining series are shown in Figure 4 and Table 4. The recorded information shows good repeatability despite the typical scarcity of the results in tests with this kind of materials. The three previously described stages can be observed clearly in most of the curves. Table 4 includes the classic tensile strength, the Young's modulus of stage III, and the final strain of each stage. The tensile stress of the specimens was calculated dividing measured load by the area of internal reinforcement: $b \cdot t_f \cdot n$, where b is the width of the specimen (100mm), t_f is the design thickness (0.0349mm) and n is the number of textile layers installed as internal reinforcement.

Fig. 4. Load-strain behaviour of reinforced specimens.

Table 4
Average results for each TRM series

The failure mode changed from one series to another. While specimens reinforced with one single textile fabric broke smoothly, the increase of the reinforcing ratio turned the failure mode into a more brittle rupture, i.e. a sudden loss of bearing capacity. The crack pattern developed is also different and this might be attributed to the fact that the specimen with one layer does not have the minimum amount of reinforcement to behave as a composite material.

The development of the value of the Young's modulus in Stage III is a key aspect in the study of this composite. In series TB1, its average value was 43GPa while in the series reinforced with two to four basalt layers the average values remained close to 60GPa. The commented low amount of internal reinforcement in series TB1 can be an explanation for this discrepancy. Something similar can be observed for the tensile strength; series TB2, TB3 and TB4 had similar average tensile strength. There was good correlation in these three series in terms of the Young's modulus, tensile strength, and ultimate strain. The main difference was observed in the development of stage II, the multiple cracking stage. Its length was reduced with a higher number of reinforcement

layers. This effect, also observable in reinforced concrete, has been reported in previous works [23].

It has been remarked in the Introduction that the stiffness of this third stage is lower than the elastic modulus of the textile reinforcement. The textile Young's modulus is 67GPa so there is a reduction around the 10%.

The increase of the reinforcement rate also affected the crack pattern, which strongly influenced the behaviour of the composite. The number of cracks was higher with more number of basalt textiles acting as strengthening core (see Fig. 5). Besides, the distance between cracks was reduced as well as their width. The reduction of the length of stage II is directly related to the formation of more cracks.

Fig. 5. Crack pattern in different specimens.

Another important remark is the loss of stiffness prior to the rupture strain. This effect could be caused by debonding at the interface textile-matrix. A further explanation is the progressive rupture of filaments inside the rovings [17]. The fracture propagates slowly in the neighbouring bundles, resulting in a failure mechanism that may be considered as ductile compared with FRP under uniaxial tensile load [24].

5. TRM modelling

For the modelling of TRM, two different approaches are presented. In the first model, the authors present the Aveston-Cooper-Kelly theory (ACK) and, in the second approach the TRM samples are simulated performing a non-linear finite element analysis (FEA). Finally the results of the TRM modelling are compared with the experimental tests.

5.1. ACK-Theory

The Aveston-Cooper-Kelly theory was developed to define a theoretical stress-strain behaviour of a composite with a brittle matrix, in which the fibre-matrix bond remains intact after the matrix has cracked [25, 26]. The extent of fibre debonding and crack spacing in a partially debonded composite are closely linked to the maximum shear stress at the fibre-matrix interface.

Several authors have already modelled multiple cracking in brittle matrix composites basing their model on the ACK theory, e.g. [27], [28] or [29]. Basic assumptions, employed in the development of the ACK theory are:

- The fibres are only capable of carrying load along their longitudinal axis.
- The matrix-fibre bond is weak.
- Once the matrix and the fibre are debonded, a pure frictional shear stress τ rules the matrix-fibre interface behaviour.

- The frictional interface shear stress τ is constant along the debonded interface.
- Poisson effects of the fibre and matrix are neglected.
- Global load sharing is assumed for the fibres.
- Normal matrix stresses, transversal to the loading direction, are uniform in a cross section.

Fig. 6. Typical stress-strain curve of TRM in tension (in grey) and ACK theory (in dotted black)

As has been previously stated, TRM tensile behaviour could be divided in three different, but complementary stages. The ACK theory model reproduces this behaviour by means of three straight lines which superimpose the experimental stress-strain curve (see Fig. 6). According to ACK theory, in the first stage, the composite obeys the law of mixtures:

$$E_{t,I} = E_f V_f + E_m V_m \quad (1)$$

where $E_{t,I}$ is the composite stiffness, V_f and V_m are the volume fraction of the fibre and matrix, respectively. E_f represents the stiffness of the fibres, whereas E_m is the matrix stiffness. At this stage, the matrix-fibre interface is assumed to be elastic.
Stage I is completed when a determinate tensile failure stress, σ_{mc}, is reached. At this value, which is directly influenced by the mortar's tensile failure stress σ_{mu}, the composite presents multiple cracking.

$$\sigma_{mc} = \frac{E_{t,I}\sigma_{mu}}{E_m} \quad (2)$$

When a crack appears in the matrix and reaches a fibre, debonding of the matrix-fibre interface occurs due to weakness at this point. Then a constant frictional interface shear stress τ is assumed. This shear stress provides normal stress transfer from fibres to the inorganic matrix. The length of the debonded interface δ can be written by expressing the force equilibrium along the loading (longitudinal) axis of the fibres [25]:

$$\delta = \frac{V_m r \sigma_{mu}}{V_f 2\tau} \quad (3)$$

where, r is the fibre radius and τ is the frictional matrix-fibre shear stress. At the multiple cracking stage, distances between cracks are no smaller than δ and no larger than 2δ. The spatial introduction of cracks occurs randomly until no space remains for new cracks, in a similar way to the geometrical car parking problem. Widom determined that the average distance between cracks equals X=1.337δ [30]. For this value, the composite strain at the end of stage II ($\varepsilon_{t,II}$) can be defined as:

$$\varepsilon_{t,II} = (1 + 0.666\alpha_e)\frac{\sigma_{mu}}{E_m} \quad (4)$$

where:

$$\alpha_e = \frac{E_m V_m}{E_f V_f} \quad (5)$$

After $\varepsilon_{t,II}$ is reached and multiple cracking has stopped, the matrix stresses remain constant with increasing the applied external load. During the final stage, only fibres contribute to bear load. The composite stiffness at this stage is defined by:

$$E_{t,III} = E_f V_f \quad (6)$$

The data necessary to run the ACK model is included in sections 2 and 3 of this paper:

- E_f: 67GPa
- E_m: 8.25GPa
- t_f: 0.0369mm
- σ_{mu}: 2.48MPa

Table 5 is completed according expressions 1 to 6 and the previous data. Moreover, the stress-strain relationship obtained by employing the ACK model is directly compared with the experimental results in Figure 7.

Table 5
ACK Theory results

Fig. 7. ACK model in series TB1 to TB4

5.2.Modelling with a 3D FEA

The Finite Elements Analysis (FEA) is a 3D powerful tool for material modelling and analysis of structural responses. In the present study, the FEA method was used in order to model the TRM under tension.

5.2.1. Material modelling

The finite element analysis was conducted with a finite element code developed by Cervenka [31]. The FEA includes realistic constitutive model of concrete behaviour that allows a simulation of the real structure behaviour in service as well as in ultimate loading conditions. The numerical model was based on three-dimensional isoparametric elements with eight nodes except for the steel tab element where brick-tetra elements

were used. In order to obtain a model with a reasonable number of finite elements (without losing too much time during the analyses and using a refined mesh), only one half of the specimens was modelled using symmetry.

The code is highly directed to reinforced concrete structures and no specific constitutive law is available for mortars. However, constitutive laws for mortars were assumed as same for concrete in order to model, as close as possible, the mortar non linear behaviour. The material chosen to simulate mortar was CC3DNonLinCementitious2 [31], which consists in a combined fracture-plastic model for concrete. When mortar is under tension the fracture model is based on the classical orthotropic smeared crack formulation and the crack band approach. It employs the Rankine failure criterion, exponential softening, and it can be used as a rotated or a fixed crack model [32]. In present work, it was assumed the rotated crack model until 40% of the tensile strength of the mortar followed by the fixed crack. This criterion was assumed based on the conveniences and inconveniences that pure fixed or rotated crack provides the model [31]. For instance, assuming a fixed crack model will result in a more rigid model when compared to reality, and assuming a rotated crack model it is impossible to reproduce in the reality because the crack orientation cannot change with the load increments applied to the structure [32].

The FE code provides softening laws to simulate crack formation in the crack process zone (CPZ) where the stresses decrease on the cracked face. Afterwards, cracking is governed by non-linear fracture mechanics. The crack bond model is considered to control the localization of deformations at failure. In this model the material parameters are adjusted such that the same amount of energy is dissipated during failures of a large and small finite element [33]. In the final, the structure modelled shows weak mesh sensitivity and the nonlinearities of the mortar (e.g. crack pattern and crack initiation/development) are approximated as close as possible to the reality.

Decrease of compressive strength in the cracked concrete is also considered and the hardening/softening plasticity model of the concrete compressive state is based on the failure surface of Menétrey–William [34]. More details can be found in [31].

Basalt fibres were modelled by discrete bar elements, and each one were defined by a uniaxial stress-strain relationship according to the tests previously performed and included in Section 2. These discrete bar elements work as truss elements, i.e. only normal stresses (tension/compression) are considered. The bond-slip models associated to basalt-to-mortar interface were considered based on some models presented in [35]. The results obtained for the TB4 series (with four layers of basalt) are presented in Table 6. The results showed no significant deviations between the models with bond-slip laws and the model with a rigid mortar-to-basalt interface. Therefore, the rigid bond interface between basalt and mortar was assumed in all specimens.

Table 6
FE code results obtained in the series TB4 assuming a bond-slip model in the mortar-to-basalt interface.

The load applied to the specimens was simulated by a regular prescribed displacement in each step of 0.02mm/step and the resulting stresses, strains, deformations, cracks, etc. satisfies the equilibrium of forces, compatibility of deformations and material laws for each step analysed due to the standard convergence criteria defined in the FE code [31]. All iteration process is governed by the Newton-Raphson method.

5.2.2. Finite element mesh

The adopted dimensions were the same that those used in the tested samples. By means of symmetry, only one half of each specimen was modelled in order to simplify the calculation process of the software. In total, 2340 FE and 3084 nodes were used.
The mortar element is characterized by brick elements with 5x5x5mm^3. In the 10mm of the thick specimen, two FE were used and ten FE were distributed along the 50mm of the one half of the specimen width.
As in the experimental specimens, reinforcement was incremented in two textile layers at both ends of the specimens in order to promote their failure in the middle portion and avoid the premature rupture near the gripping devices. This feature was also considered in the FEA and, therefore, the extra reinforcements were introduced in the model.

6. Analysis and discussion of results

The results of the presented ACK theory and FEA are directly contrasted with the experimental data in Figure 8. Throughout this point the obtained data is analysed and discussed. In order to facilitate a clear understanding of the graphs, the area covered by the experimental curves is highlighted in grey while the numerical curve is represented in black colour. This information is also summarized in Table 7.

Fig. 8. ACK theory and FEA series TB1 to TB4.

The ACK model presents interesting results compared to the experimental data. In general terms, mainly at stage III, this model proved to be less than fully effective. The main discrepancy point is the value for the end of the multi-cracking stage, ε_{mc}. Besides, the stiffness of the third stage appears to be greater in the model. This discrepancy is caused by the loss of stiffness observed at the end of stage III in all the tested combinations. The progressive rupture of filaments inside the rovings [17] and the debonding at the textile-matrix interface could be the main reasons for this loss of stiffness. The fracture propagates slowly in the neighbouring bundles, resulting in a

failure mechanism that may be considered as ductile [24]. The ACK model does not expect this behaviour.

Table 7
Comparison between average values from experimental tests and TRM modelling from ACK Theory and FEA.

Moreover, this model works better with more basalt layers. However, the lack of accuracy of the ACK model in heavily reinforced organic based composites was checked [23]. Probably, ACK theory reproduces suitable results in a specific ratio of composite internal reinforcement.

The results from the FEA model follow very closely TRM behaviour observed experimentally in terms of load vs. strain (Fig. 8). The numerical curve captures the real behaviour nicely when there is enough reinforcement material to act as a composite. For series TB1, there are several discrepancies than can not be neglected. As was remarked in the analysis of the experimental data, the composite stiffness ($E_{t,III}$) was clearly lower in series TB1 than in the remaining series. The FEA does not take into account the problems derived from the lack of internal reinforcement ratio and produces a curve that shows considerable differences with the experimental ones. In fact, the value $E_{t,III}$ obtained in the FEA, 64.5MPa, is very similar to those recorded experimentally in series TB2, TB3 and TB4.

The proposed simulation presents optimum results for the multiple cracking strain, $\varepsilon_{t,II}$. There are no significant discrepancies between the analytical and experimental data on this key point.

The behaviour of the model at stage III is not completely satisfactory. There is agreement on the first phase of this stage. However, as strain increases and approaches to the rupture point, there are some differences between the model and the experimental curves that could be justified by two distinct facts: i) the basalt rovings were modelled by discrete bar elements corresponding to a unique element that models an enormous number of basalt filaments. When basalt ultimate strain is reached, the roving collapses in a brittle way in the numerical simulation. From the experiments and bibliography [17,23], it was noticed a progressive rupture of several filaments before the whole specimen collapses; ii) the failure is based on the linearity of the model caused, independently of the bond-slip law considered for the basalt-to-mortar interface, by the assumption of no slips can occur at both ends of the basalt roving [23].

Fig. 9 presents the smeared cracking pattern of the one half of the TB3 model. The results show that there are higher principal strains developing in the area without the extra reinforcements used to avoid a premature rupture and focus the development of cracks in the measured area.

Due to this lack of convergence at the rupture stage, the estimation of the maximum uniaxial tensile strength disagrees slightly with the average experimental value (see Table 7).

Fig. 9. Crack pattern developed by FEA model (TB3) before the first crack appeared (a) and at failure moment (b).

The analysis of the results (see Fig. 8) reveals that the overall behaviour of the TRM load-strain curves are not significantly affected by the interface between basalt fibres and mortar, i.e. the global behaviour of the specimens under tension is independent of the bond-slip curve chosen. Let us discuss this mechanism in some more detail.

During Stage I, all materials have an elastic response. On such circumstances and from the longitudinal load equilibrium in an infinitesimal length dx, the bond stresses can be determined at the filament level according to (e.g. [36]):

$$\tau(x) = E_f \cdot \frac{\phi_f}{4} \cdot \frac{d\varepsilon_f}{dx} \tag{7}$$

where Φ_f is the diameter of the basalt filaments; ε_f is the strain of the basalt; and x is the coordinate associated to the bonded length.
The slippage of the interface can be calculated as:

$$s = u_f - u_m \tag{8}$$

where u_f and u_m are, respectively, the displacements of the basalt filaments and the displacements of the mortar. Differentiating (8) in order to x:

$$\frac{ds}{dx} = \frac{du_f}{dx} - \frac{du_m}{dx} \tag{9}$$

where du_f/dx and du_m/dx are, respectively, the strains of the basalt filament and the strains of the mortar. Eq. (7) can be rewritten as:

$$\tau(x) = E_f \cdot \frac{\phi_f}{4} \cdot \frac{d\varepsilon_f}{ds} \cdot \frac{ds}{dx} \tag{10}$$

and replacing Eq. (9) in Eq. (10), the bond stresses can be determined according to:

$$\tau(x) = E_f \cdot \frac{\phi_f}{4} \cdot \frac{d\varepsilon_f}{ds} \cdot (\varepsilon_f - \varepsilon_m) \tag{11}$$

In general, the $\varepsilon_f(s)$ is a nonlinear function that can be determined experimentally [35]; however, for low loads, $\varepsilon_f(s)$ can be represented by a linear function and so, $d\varepsilon_f/ds$ is constant. Again, for low loads, the strains in the basalt filaments and strains in the mortar are low and similar. Consequently, bond stresses can be assumed equal to zero. This justifies the insensibility of different bond-slip curves verified in the FEA in Stage I (see Table 7). In fact no significant differences were found for maximum strain or stresses in this stage when different bond-slip curves were assumed in the FEA.

The plateau observed on Stage II is due to the initiation, development and stabilization of the cracks in the mortar. Thus, the bond-slip curves have no influence at this stage.

As load increases in Stage III, the load transmitted to the basalt filaments also increases and the slippages can occur in the basalt-to-mortar interface. However, due to the short spacing between cracks, the maximum loads that can be transmitted to the basalt filaments are very low (bonded length is very smaller than the effective bond length, e.g. [37-39]) and the basalt-to-mortar interface collapses for low loads. Also for the same reason, Stage III has a similar stiffness to that observed from the tensile tests of the basalt filaments. Again, no significant influence on the global behaviour was observed in the TRM tensile tests when a bond-slip curve was assumed to model the basalt-to-concrete interface. However, a more detailed observation of the stress-strain curve obtained from the TRM tensile tests reveals that the stiffness in Stage III is slightly lower than that observed from the tensile test of the basalt filaments. This observation can be justified by the slippages of the basalt-to-mortar interface located within the tabs of the specimens.

For all the reasons exposed above, the basalt-to-concrete interface was assumed to be rigid in the FEA. Moreover, assuming a rigid interface, the number of finite elements of the model did not increase unnecessarily and the solution of the FEA did not consume so much time.

7. Conclusions

The data obtained in the TRM uniaxial tensile contribute to a better understanding of the behaviour of this composite material. The procedure retained for TRM characterisation in tensile proved effective. Good repeatability was observed between the stress-strain curves. The reinforcement ratio, as a basic parameter, is broadly

studied. Moreover, in the present paper, basalt is presented as a possible material for reinforcing or strengthening applications.

The basalt TRM has a non-linear behaviour into three stages. The first one is controlled by the stiffness of the mortar. The second stage is characterized by a multiple cracking stage and begins when the mortar tensile strength is exceeded, and continues with the equilibrium between the tensile in the mortar and in the basalt textile. When all the cracks are formed, the third stage begins with the material in a linear way, controlled by the E-modulus of the basalt textile until its rupture.

The Finite Element Analysis (FEA) proves to be a good way to simulate the TRM in tension due to its good correlation with the experimental data. The basalt-to-mortar interface can be modelled as a rigid interface. The inclusion of bond-slip curves into the FE code did not improve the global response of the TRM tensile tests. Therefore, the assumption of rigid interface was sufficient to estimate, with a good accuracy, the three stages observed in the experiments.

In addition, a well-known model as ACK theory is also included in this document and its simulations compared with the experimental results. Both ACK and the FEA estimate with good accuracy the tensile behaviour of the TRM tests.

It is very important to simulate accurately the failure mode of the composite. But, there are strengthening applications where TRM is not expected to reach so high strains. For example, for reinforced concrete flexural strengthening it is mandatory that the steel reinforcement strain remains lower than 1%. Thus, TRM strain may work in the vicinities of that value where the correlation between the experimental data and the numerical model is more accurate.

The numerical model presented and calibrated here may be used for posterior modelling of reinforced concrete elements such as beams or slabs reinforced or strengthened with technical textiles.

Acknowledgments

This research work was funded through the research projects DFB 7-12-TK-2009-10 and BIA2010-20789-C04-03/04; the Basque Government's contract IT781-13; and the scholarship programme of the Iñaki Goenaga Foundation.

References

[1] Ombres L. Flexural Analysis of Reinforced Concrete Beams Strengthened With a Cement Based High Strength Composite Materials. Composite Structures 2011; 94: 143-155.

[2] Triantafillou TC, Papanicolau CG. Shear Strengthening of RC Members with Textile Reinforced Mortar (TRM) Jackets. Materials and Structures 2007; 39: 85-93.
[3] Larrinaga P, San-José JT, García D, Garmendia L, Díez J. Experimental Study of the Flexural Behaviour of Low Performance RC Beams Strengthened with Textile Reinforced Mortar. Proceedings of the International RILEM Conference on Material Science (MatSci). Aachen, Germany. 2010; Vol. 1: 235-244.
[4] Larrinaga P, San-José JT, García D, Garmendia L. Refuerzo a flexión de hormigón de bajas prestaciones mediante materiales compuestos de matriz inorgánica. Hormigón y Acero. Revista trimestral de ACHE 2012; 63-266: 79-93.
[5] Bournas D, Lontou P, Papanicolau CG, Triantafillou TC. Textile-Reinforced Mortar (TRM) versus FRP Confinement in Reinforced Concrete Columns. ACI Structural Journal, 104(6), pp. 740-748. 2007.
[6] Peled A, Bentur A. Fabric Structure and its Reinforcing Efficiency in Textile Reinforced Cement Composites. Composites: Part A 2003; 34: 107-118.
[7] Hegger J, Will N, Bentur A, Curbach M, Mobasher B, Pelled A, Wastiels J. Mechanical Behaviour of Textile Reinforced Concrete. Textile Reinforced Concrete. State-of-the-art Report of RILEM TechnicalCimittee 201-TRC 2006: 133-186.
[8] Jesse F, Will N, Curbach M, Hegger J. Load Bearing Behaviour of Textile Reinforced Behaviour. Textile Reinforced Concrete. ACI Special Publication (SP). Dubey A. (Ed.) 2008: 59-68.
[9] Jesse F. Tragverhalten von Filamentgarnen in Zementgebundener Matrix. PhD Thesis, Dresden: Fakulty of Civil Engineering, Technische Universität Dresden. 2005.
[10] Peled A, Bentur A. Geometrical Characteristics and Efficiency of Textile Fabrics for Reinforcing Cement Composites. Cement and Concrete Reseach, 2000; Vol 30, Issue 5: 781-790.
[11] Di Ludovico M, Prota A, Manfredi G. Concrete Confinement Using Innovative Materials: Basalt Reinforced Mortar (BRM). Proceedings of the Challanges for Civil Construction – CCC2008. Torres Marques et al (Eds.). FEUP, Porto, Portugal, 2008: 124-125.
[12] Borham TM. Properties of glass concrete reinforced with short basalt. Materials & Design 2012; 42: 265-271.
[13] OPERHA. Open and Fully Compatible Next Generation of Strengthening System for the Rehabilitation of Mediterranean Building Heritage. Contract no. 517765 (INCO), 6th FP. 2006-2008.
[14] Sim J, Park c, Moon DY. Characteristics of Basalt Fiber as a Strengthening Material for Concrete Structures. Composites. Part B 2005; 36: 504-512.
[15] Garmendia L, San-José JT, García D, Larrinaga P. Rehabilitation of Masonry Arches with Compatible Advanced Composite Material. Construction and Building Materials 2011; Vol 25, Issue 12: 4374-4385.
[16] Curbach M. Textile Reinforced Structures. Proceedings of the 2nd Colloquium of Textile Reinforced Structures (CTRS2), Dresden 2003; 29-9.
[17] Larrinaga P. Flexural Strengthening of Low Grade Concrete Through the Use of New Cement-Based Composite Materials. PhD Thesis, University of the Basque Country, Spain. 2011.
[18] Keil A, Cuypers H, Raupach M, Wastiels J. Study of the Bond in Textile Reinforced Concrete: Influence of Matrix and Interface Modification. Proceedings of the Challanges for Civil Construction – CCC2008. Torres Marques et al (Eds.). FEUP, Porto, Portugal. 2008.
[19] García D. Experimental and Numerical Analysis of Stone Masonry Walls Strengthened with Advanced Composite Materials. PhD Thesis, University of the Basque Country, Spain. 2009.
[20] UNE-EN 1015-11:1999. Métodos de ensayo para morteros de albañilería. Parte 11: Determinación de la resistencia a flexión y a compresión del mortero endurecido. Asociación Española de Normalización y Certificación. AENOR. 1999.
[21] Haüßler-Combe U, Hartig J. Bond and Failure Mechanism of Textile Reinforced Concrete (TRC) under Uniaxial Tensile Loading. Cement & Concrete Composites, 29, pp. 279-289. 2007.
[22] Hegger J, Voss S. Investigations on the Bearing Behaviour and Application Potential of Textile Reinforced Concrete. Engineering Structures 2008; 30: 2050-2056.
[23] Cuypers H, Wastiels J. A Stochastic Cracking Theory for the Introduction of Matrix Multiple Cracking in Textile Reinforced Concrete under Tensile Loading. Proceedings of the 1st International RILEM Symposium. RILEM Technical Committee 201-TRC. Aachen, Germany 2006: 193-202.
[24] Triantafillou TC, Papanicolau CG. Textile Reinforced Mortars (TRM) versus Fiber Reinforced Polymers (FRP) as Strengthening Materials of Concrete Structures. Proceedings of FRPRCS7 – 7th International Symposium Fiber-reinforced Polymer Reinforcement for Concrete Structures. New Orleans, USA, 2005: 99-118.

[25] Aveston J, Cooper GA, Kelly A. Single and Multiple Fracture, the Properties of Fibre Composites. Proceedings of the Conference National Physical Laboratories, IPC Science and Technology Press Ltf. London, 1971: 15-24.
[26] Aveston J, Kelly A. Theory of Multiple Fracture of Fibrous Composites. J. Mat. Sci. 1973; 8: 411-461.
[27] Curtin WA. Stochastic Damage Evolution and Failure in Fibre-Reinforced Composites. Advances in Applied Mechanics 1999; 36: 163-253.
[28] Da Silva ARC. Probabilistic Approach to Predict Cracking in Lightly Reinforced Microconcrete panels. Journal of Engineering Mechanics 2004; 8 (130): 931-941.
[29] Mobasher B, Pahilajani J, Peled A. Analytical Simulation of Tensile Response of Fabric Reinforced Cement Based Composites. Cement and Concrete Composites 2006; 28: 77-89.
[30] Widom B. Random sequential addition of hard spheres to a volume. J. Chem. Phys 1966; 44: 3888-3894.
[31] Cervenka V, Jendele L, Cervenka J. ATENA Program Documentation – Part 1 – Theory. Cervenka Consulting, Prague. May: 2009.
[32] Faria D, Biscaia HC, Lúcio V and Ramos P. Material and geometrical parameters affecting punching of reinforced concrete flat slabs with orthogonal reinforcement. IABSE-FIB Conference Cavtat, Dubrovnik-Neretva County, Croatia, May 3-5, 2010.
[33] Cervenka J, Bazant ZP, Wierer M. Equivalent localization element for crack band approach to mesh-sensitivity in microplane model. International Journal for Numerical Methods in Engineering 2005; 62: 700-726.
[34] Menétrey P, William KJ. Triaxial failure criterion for concrete and its generalization. ACI Structural Journal 1995; Vol. 92(3): 311-318.
[35] Biscaia H, Chastre C, Silva MAG. Linear and nonlinear analysis of bond-slip models for interfaces between FRP composites and concrete. Composites: Part B Journal 2013; Vol.45 (1): 1554-1568.
[36] De Lorenzis, Nanni A. Bond Between Near Surface Mounted FRP Rods and Concrete in Structural trengthening. ACI Structures Journal 2002; Vol. 99 (2): 123-133.
[37] Neubauer U, Rostásy FS. Design aspects of concrete structures strengthened with externally bonded CFRP-plates. In: Proceedings of the 7th international conference on structural faults and repairs 1997; 2: 109-118.
[38] Teng JG, Chen JF, Smith ST, Lam L. FRP strengthened RC structures. Chichester (England): John Wiley and Sons Ltd.; 2001.
[39] Biscaia H, Chastre C, Silva MAG. Nonlinear numerical analysis of the debonding failure process of FRP-to-concrete interfaces. Composites Part B: Engineering 2013; 50: 210-223.

Table 1
Manufacturing specifications of the basalt fibres and textile geometry

Basalt fibres	
Ultimate tensile strength, σ_{fu}	2100 MPa
Tensile elastic modulus, E_f	89 GPa
Ultimate tensile strain, ε_f	3.145 %
Density	2.75 g/cm^3
Basalt textile	
Design thickness, t_f	0.0349 mm
Opening size	25x25 mm
Weight of the dry sheet	233 g/m^2
Ultimate tensile load	4040 N
Ultimate tensile strength, σ_r	1160 MPa
Ultimate tensile strain, ε_r	1.82 %
Young modulus in tensile	67 GPa

Table 2
Mortar dosage by weight (%) and mechanical characterization

Sand (maximum grain size: 0.6mm)	60-70
Grey Cement Type II 42.5R	30-40
Redispersable Resins	1-3
Polymeric Chopped Fibres	3-5
Water/Cement relationship	0.2
Compressive strength $f_{c,m}$ (7d)	8.2 MPa
Compressive strength $f_{c,m}$ (28d)	21.6 MPa
Flexural strength $f_{ct,m}$ (7d)	3.5 MPa
Flexural strength $f_{ct,m}$ (28d)	8.2 MPa

Table 3
Average results of unreinforced specimens

σ_{mu} [1] (MPa)	ε_{mu} (%)	E_m (GPa)
2.48	0.03	8.25

[1] $\sigma_{mu} = F_{mu} / (10 \cdot 100)$

Table 4
Average results for each TRM series

Series	F_{tr} (N)	σ_{tr} [1] (MPa)	$E_{t,III}$ (GPa)	$\varepsilon_{t,I}$ (%)	$\varepsilon_{t,II}$ (%)	$\varepsilon_{t,III}$ (%)
TB1	3797	1088	43	0.034	0.40	2.15
TB2	8772	1256	59	0.041	0.29	1.96
TB3	12515	1195	57	0.028	0.21	2.10
TB4	16679	1194	61	0.028	0.15	2.07

[1] $\sigma_{tr} = F_{tr} / (0.0349 \cdot 100 \cdot n)$

Table 5
ACK Theory results

Series	V_m (-)	V_f (-)	$\varepsilon_{t,I}$ (GPa)	σ_{mc} (MPa)	$\varepsilon_{t,II}$ (%)
TB1	0.9965	0.0035	8.46	2.54	0.734
TB2	0.9930	0.0070	8.66	2.60	0.381
TB3	0.9895	0.0105	8.87	2.67	0.263
TB4	0.9860	0.0140	9.07	2.73	0.204

Table 6
FE code results obtained in the series TB4 assuming a bond-slip model in the mortar-to-basalt interface.

Bond-slip model		$\varepsilon_{t,I}$ (%)	$F_{t,I}$ (kN)	$\varepsilon_{t,II}$ (%)	$F_{t,II}$ (kN)	$\varepsilon_{t,III}$ (%)	$F_{t,III}$ (kN)
Rigid		0.04	2.7	0.19	2.9	2.12	19.7
Rigid-plastic	τ_{max} [1] =2MPa	0.04	2.7	0.19	2.9	2.12	19.7
	τ_{max} [1] =22MPa	0.04	2.7	0.18	2.9	2.00	18.9
Rigid softening	τ_{max} [1] =12MPa s_{ult} [2] =5μm	0.04	2.7	0.19	2.9	2.09	19.7
	τ_{max} [1] =12MPa s_{ult} [2] =5mm	0.04	2.7	0.19	3.0	1.99	18.8
Popovics's formula (nonlinear)	τ_{max} [1] =12MPa s_{max} [3] =0.5m	0.03	2.7	0.19	3.1	2.05	19.7
	τ_{max} [1] =2MPa s_{max} [3] =0.5mm	0.03	2.8	0.17	3.0	1.94	19.8

[1] maximum bond stress; [2] ultimate slip; [3] slip at maximum bond stress

Table 7
Comparison between average values from experimental tests and TRM modelling from ACK Theory and FEA.

Series	Properties	Experimental	FEA	ACK
TB1	End multiple cracking stage, $\varepsilon_{t,II}$ (%)	0.40	0.43 (7.50%)	0.73 (82.5%)
	Ultimate load, F_t (N)	3797	5650 (48.8%)	5852 (54.1%)
	Post-cracking stage Young's Modulus, $E_{t,III}$(GPa)	43	64.5 (50.0%)	67[1]
	Ultimate strain, $\varepsilon_{t,III}$ (%)	2.15	2.08 (-3.26%)	2.15[2]
TB2	End multiple cracking stage, $\varepsilon_{t,II}$ (%)	0.29	0.29 (0.00%)	0.38 (31.0%)
	Ultimate load, F_t (N)	8772	10024 (14.3%)	9988 (13.8%)
	Post-cracking stage Young's Modulus, $E_{t,III}$(GPa)	59	64.8 (9.8%)	67[1]
	Ultimate strain, $\varepsilon_{t,III}$ (%)	1.96	1.99 (1.5%)	1.96[2]
TB3	End multiple cracking stage, $\varepsilon_{t,II}$ (%)	0.21	0.21 (0.0%)	0.26 (23.8%)
	Ultimate load, F_t (N)	12515	13684 (9.3%)	15550 (24.2%)
	Post-cracking stage Young's Modulus, $E_{t,III}$(GPa)	57	64.1 (12.5%)	67[1]
	Ultimate strain, $\varepsilon_{t,III}$ (%)	2.10	1.89 (-10.0%)	2.10[2]
TB4	End multiple cracking stage, $\varepsilon_{t,II}$ (%)	0.15	0.17 (13.3%)	0.20 (33.3%)
	Ultimate load, F_t (N)	16679	17720 (6.2%)	20177 (20.9%)
	Post-cracking stage Young's Modulus, $E_{t,III}$(GPa)	61	63.7 (4.4%)	67[1]
	Ultimate strain, $\varepsilon_{t,III}$ (%)	2.07	1.86 (-10.1%)	2.07[2]

[1] textile Young's modulus; [2] experimental values are used as ultimate strain

Figure1

Click here to download high resolution image

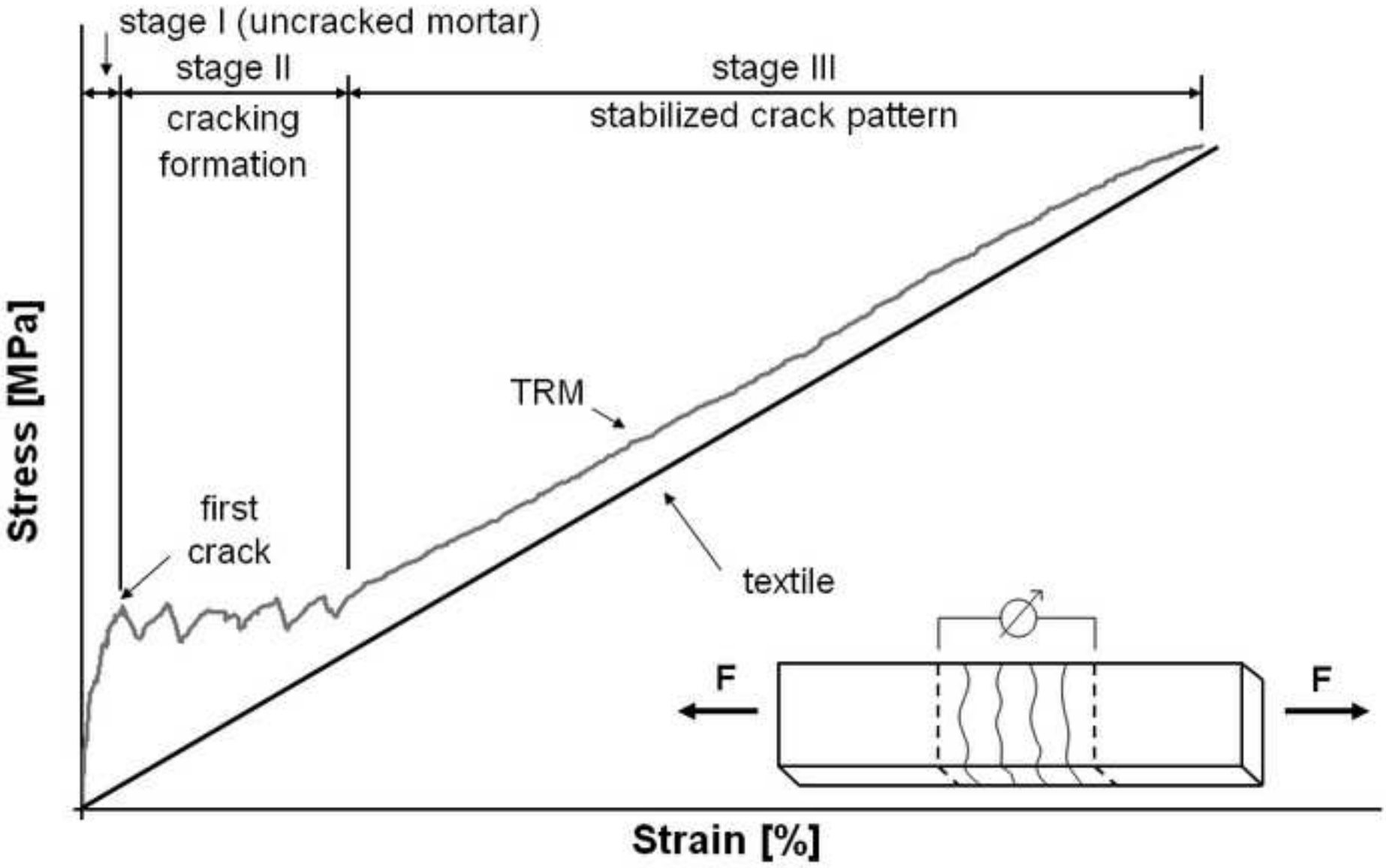

Figure2

Click here to download high resolution image

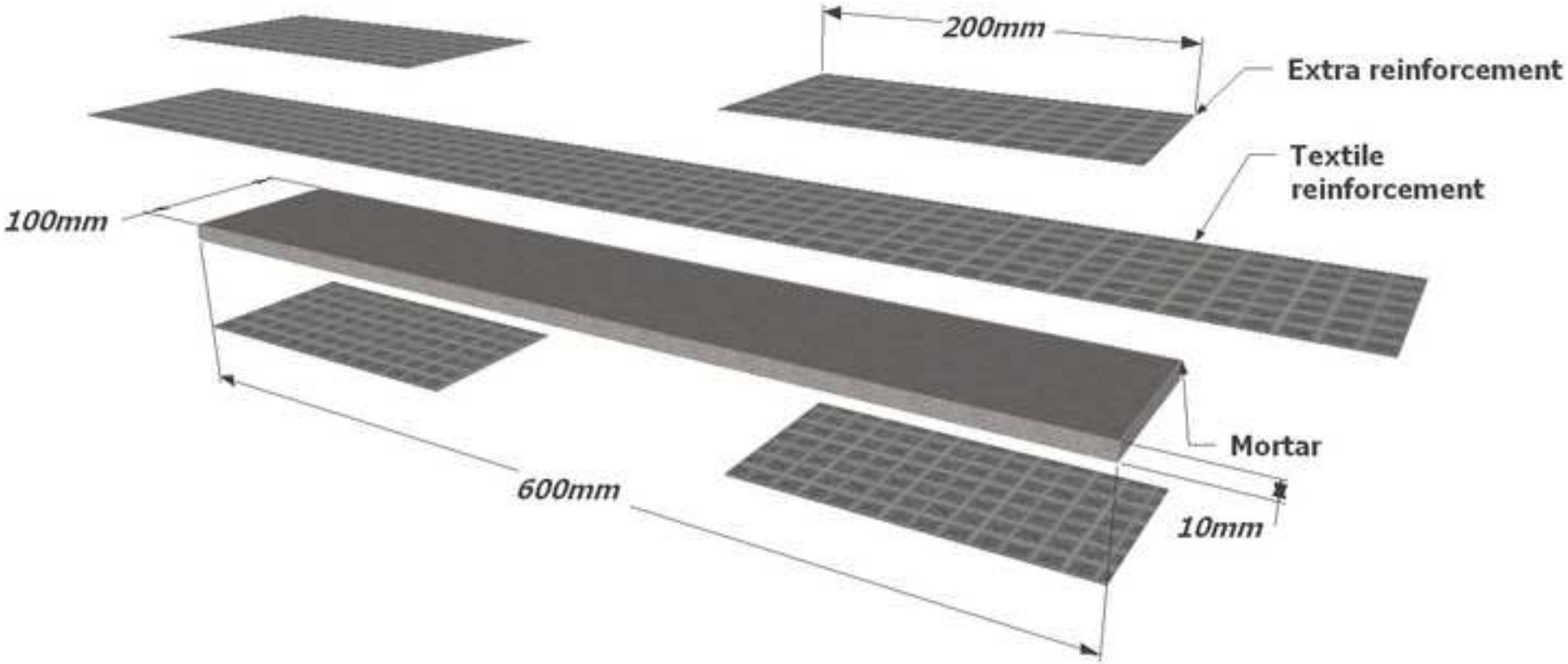

Figure3

Click here to download high resolution image

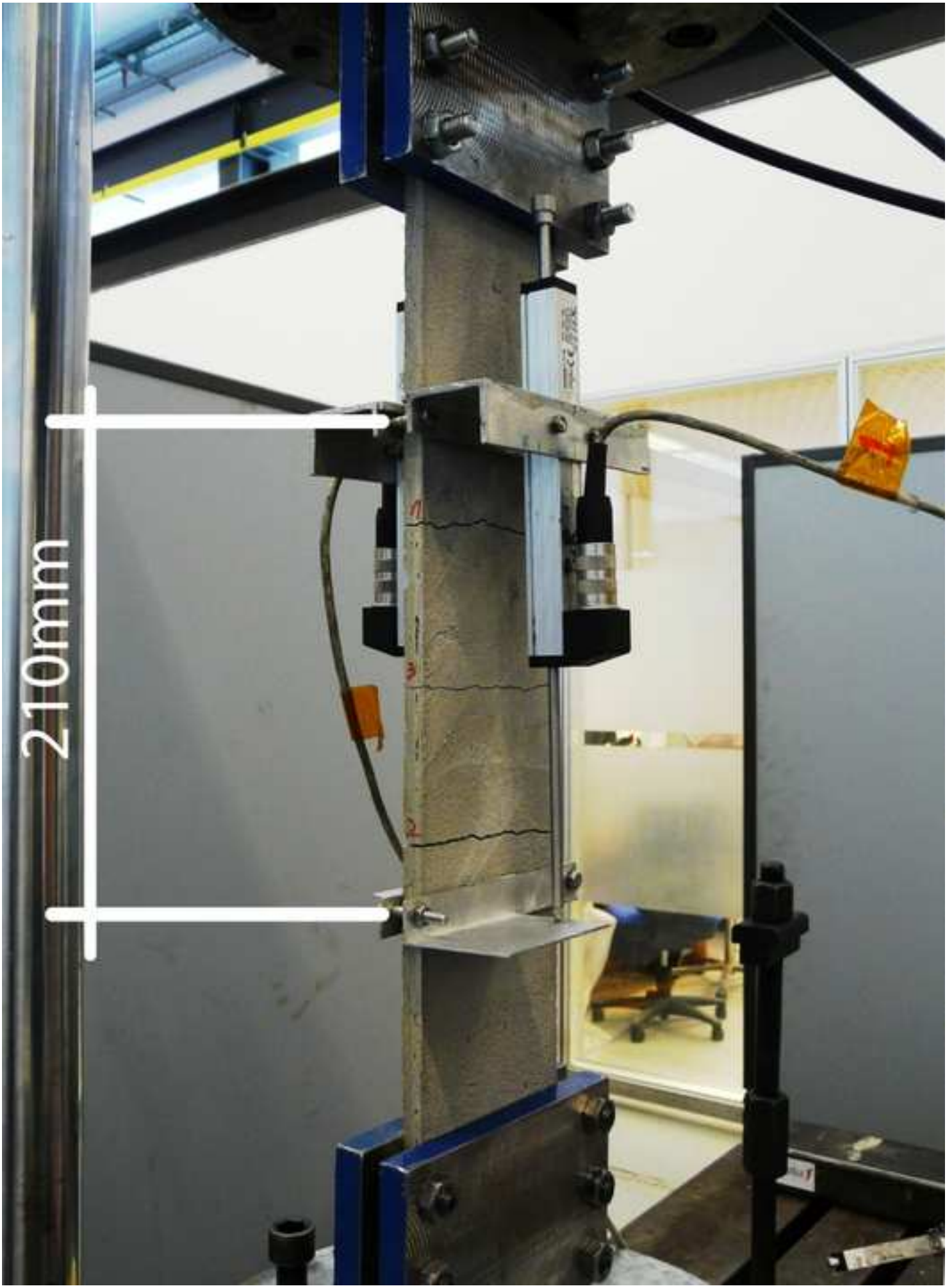

Figure4
Click here to download high resolution image

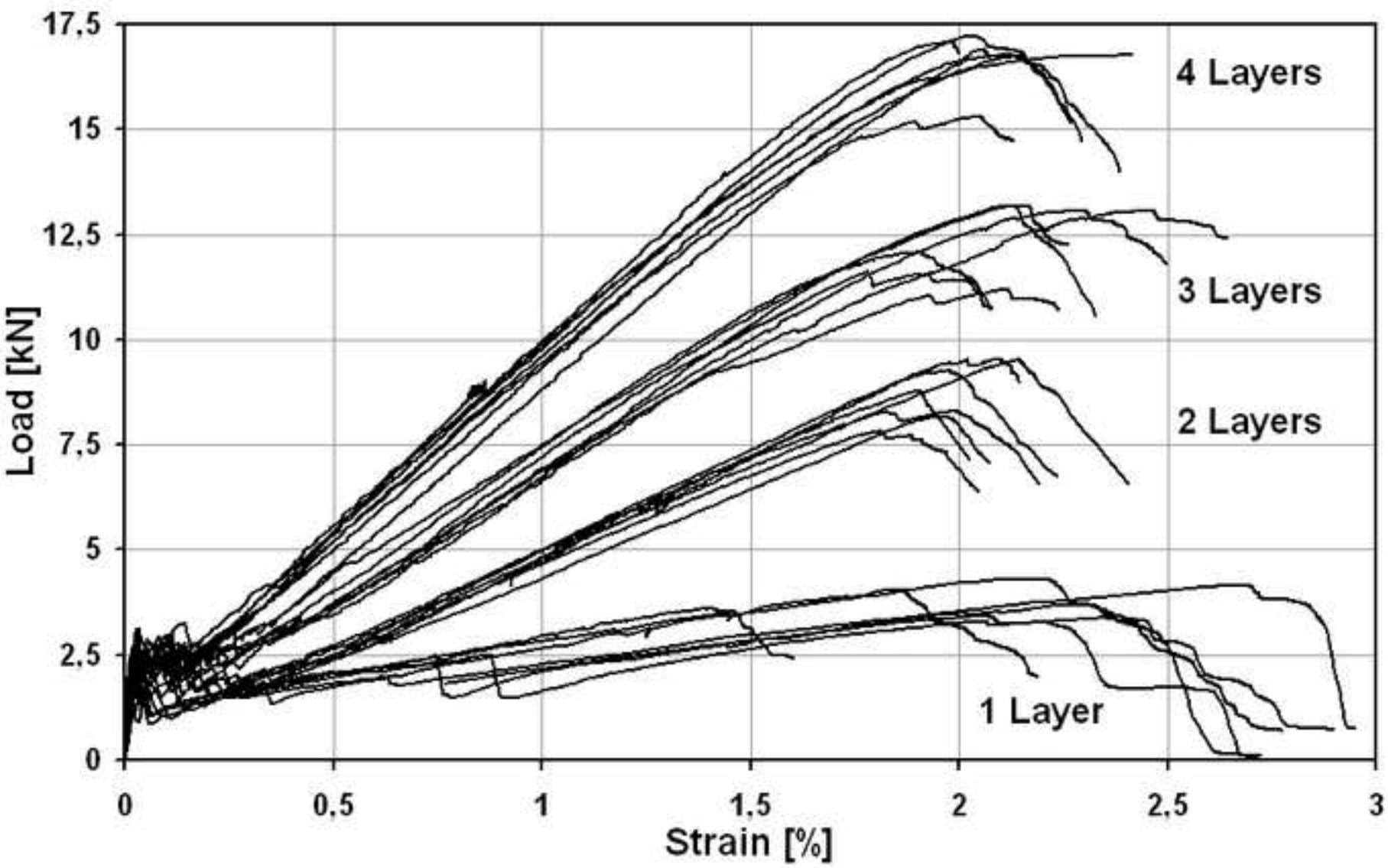

New Figure 5

Click here to download high resolution image

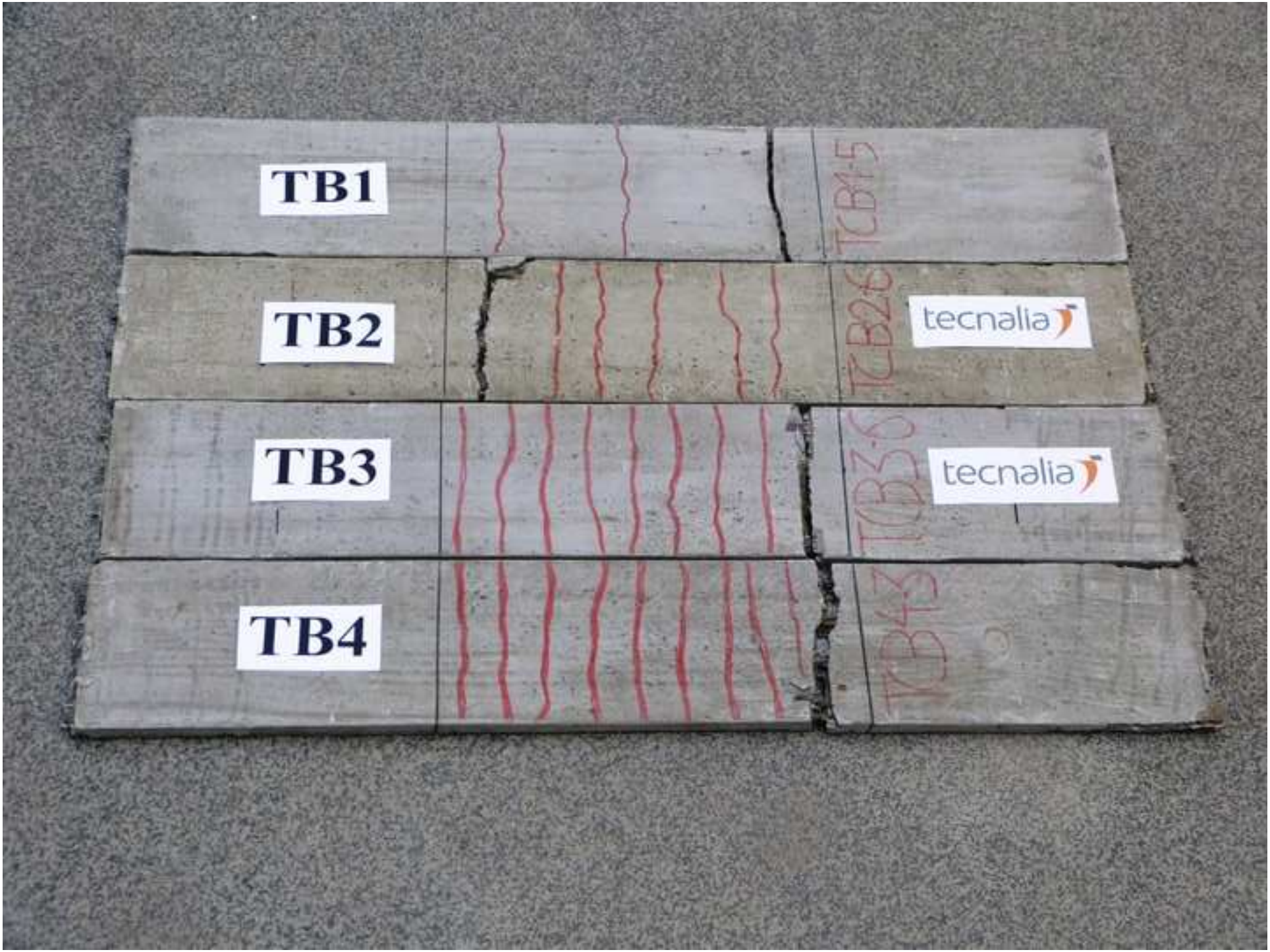

New Figure 6
Click here to download high resolution image

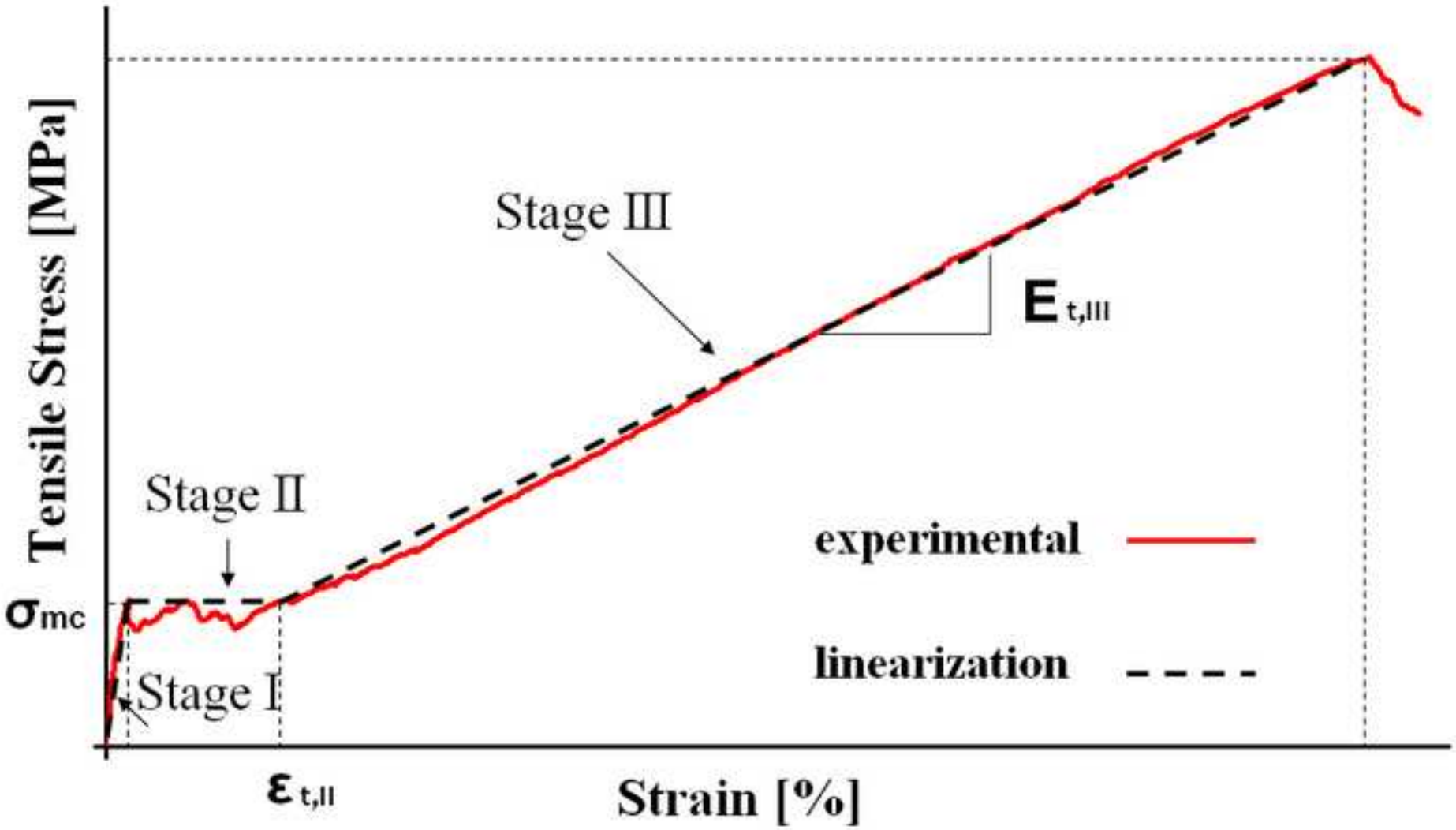

New Figure 7
Click here to download high resolution image

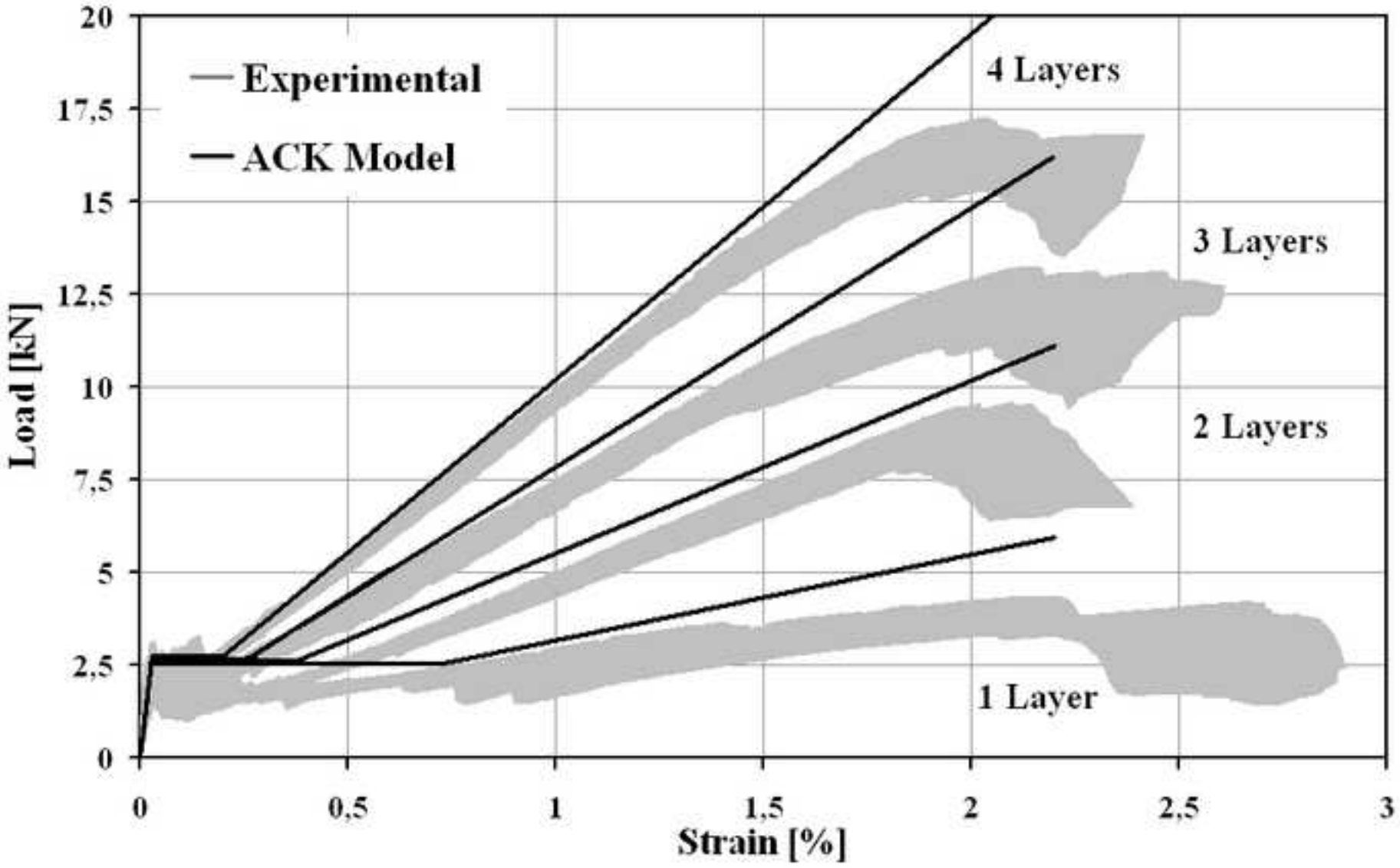

New Figure 8
Click here to download high resolution image

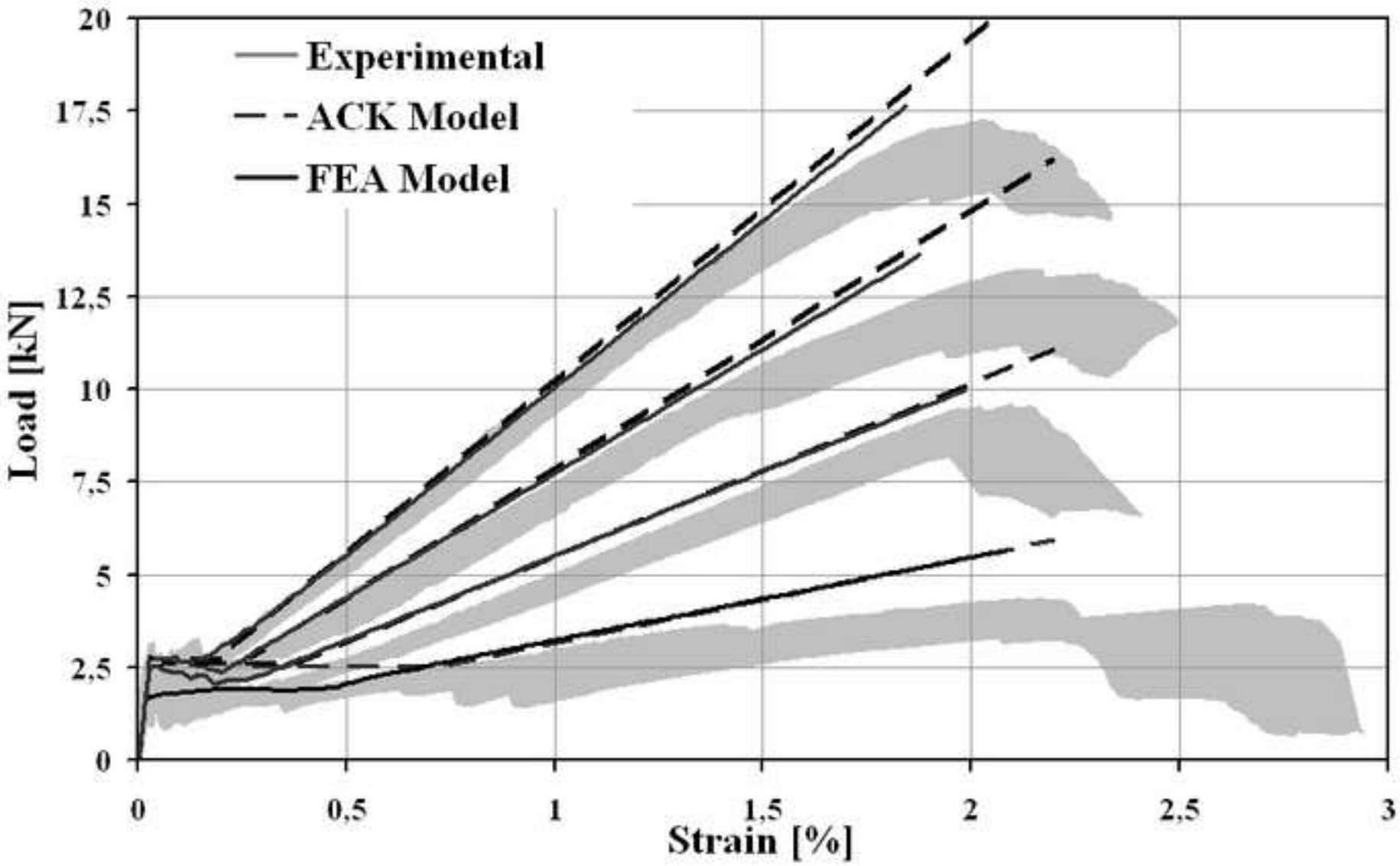

New Figure 9
Click here to download high resolution image